Lab on a Chip

PAPER

View Article Online
View Journal | View Issue

Cite this: *Lab Chip*, 2023, **23**, 2257

A multiscale, vertical-flow perfusion system with integrated porous microchambers for upgrading multicellular spheroid culture†

Mai Takagi, Masumi Yamada, * Rie Utoh and Minoru Seki

Received 28th February 2023,
Accepted 27th March 2023

DOI: 10.1039/d3lc00168g

rsc.li/loc

Spheroid formation assisted by microengineered chambers is a versatile approach for morphology-controlled three-dimensional (3D) cell cultivation with physiological relevance to human tissues. However, the limitation in diffusion-based oxygen/nutrient transport has been a critical issue for the densely packed cells in spheroids, preventing maximization of cellular functions and thus limiting their biomedical applications. Here, we have developed a multiscale microfluidic system for the perfusion culture of spheroids, in which porous microchambers, connected with microfluidic channels, were engineered. A newly developed process of centrifugation-assisted replica molding and salt-leaching enabled the formation of single micrometer-sized pores on the chamber surface and in the substrate. The porous configuration generates a vertical flow to directly supply the medium to the spheroids, while avoiding the formation of stagnant flow regions. We created seamlessly integrated, all PDMS/silicone-based microfluidic devices with an array of microchambers. Spheroids of human liver cells (HepG2 cells) were formed and cultured under vertical-flow perfusion, and the proliferation ability and liver cell-specific functions were compared with those of cells cultured in non-porous chambers with a horizontal flow. The presented system realizes both size-controlled formation of spheroids and direct medium supply, making it suitable as a precision cell culture platform for drug development, disease modelling, and regenerative medicine.

Introduction

Maximizing the functionality of mammalian cells is crucial for cell-based drug evaluation and the creation of bioartificial organs. Accordingly, *in vitro* systems that can reproduce human tissue-relevant conditions are in great demand. Cell cultures using three-dimensional (3D) platforms have proven to be highly effective for maintaining cell viability and inducing proper cell function, polarity, and differentiation. For the past decade, formation of multicellular clusters known as spheroids has been among the most popular strategies for 3D cell culture.[1–4] Control of stem cell differentiation has been achieved using tissue-like organoids that can recapitulate the developmental fields of multicellular organoids.[5,6] To better model the responses of cells to drug candidates, organotypic multicellular spheroids have also been created.[7–9] In spheroid culture platforms, expressions of integrins and cadherins involved in cell–cell and cell–matrix interactions are enhanced compared to those in 2D plate culture.[10,11] These receptors bind to the actin cytoskeleton and subsequently regulate the downstream signal transductions from the extracellular stimuli.[12] In the fundamental process of cell homeostasis, these coordinated and dynamic responses of two or more types of receptors in spheroids are the key to the proper functioning of cells.

To date, numerous studies using spheroid culture have described the improved cell functions and ideal cell behaviors achieved in hepatocytes,[13] pancreatic islet cells,[14] neural cells,[15] cardiomyocytes,[16] and osteoblasts.[17] The functions of cells within the spheroids have been further upregulated through the control of spheroid size,[14,18] the introduction of multiple cell types,[19] and the hierarchical assembly of spheroids.[20,21] Additionally, incorporation of microengineered biomaterials, especially microparticles and microfibers composed of extracellular matrix components, has been shown to be highly effective in enhancing the cell–matrix interactions within spheroids.[22–24]

Typical methods of forming spheroids include, but are not limited to, the use of non-cell-adherent dishes,[25] hanging drop method,[26] rotational cultures,[27] and microfabricated chambers.[22,28,29] Among these techniques, microchamber-based cultivation is the most capable of precisely controlling the spheroid size and morphology in a high-throughput manner without necessitating complicated operations and

Department of Applied Chemistry and Biotechnology, Graduate School of Engineering, Chiba University, 1-33 Yayoi-cho, Inage-ku, Chiba 263-8522, Japan. E-mail: m-yamada@faculty.chiba-u.jp; Tel: +81 43 290 3398

† Electronic supplementary information (ESI) available: Supplementary Fig. S1–S5 and Movie S1. See DOI: https://doi.org/10.1039/d3lc00168g

devices. Despite its many successes, however, spheroid culture has several drawbacks. Most importantly, there is a limited oxygen supply to the cells composing the spheroids. The problem of hypoxia is especially severe for large spheroids, *i.e.*, those with diameters larger than ~300 μm.[30–32] In such larger spheroids, the delivery of oxygen and nutrients to and the removal of metabolized waste from the cells are also decelerated, leading to necrosis, especially in the center region of the spheroid.

Numerous attempts have been made to address the problem of oxygen/nutrient deprivation in spheroids. Microchambers with a bottom layer composed of an oxygen-permeable silicone membrane have been developed to enhance the oxygen supply.[30,33,34] Perfusion culture has also been performed as a powerful strategy for directly supplying the culture medium to the spheroids formed in microchambers.[35,36] In standard perfusion culture systems, microchambers are placed on the bottom of fluidic channel structures. Dispersed cells seeded in the chambers are precipitated by gravity, and then the spheroids are formed under the continuous introduction of the culture medium through the channel structures. The cell viability and function can be improved by refining the attributes of the medium flow.[37,38] However, the channel/chamber designs of perfusion devices often result in flow stagnation, with the streamlines failing to reach the bottom of the chambers but rather merely passing over the chambers.[39] In addition, the culture conditions are not uniform across the chambers: the downstream chambers do not grow cells as well as the upstream chambers because the metabolism by cells deprives the downstream chambers of medium components.[40] These problems are unavoidable in conventional perfusion systems, where the chambers are placed vertically at the bottom of horizontally arranged channels. Therefore, it would be desirable to configure the device in such a way that the culture medium directly flows through the chambers while the introduced cells are retained to form spheroids. We expect that such a device would provide effective culture conditions for the formation of uniform-sized spheroids, but designing such a platform is not trivial.

Recently, porous polydimethylsiloxane (PDMS)-based substrates have been utilized as functional materials with a large surface area and well-controlled porosity.[41] The applications of porous PDMS materials with continuous inner micropores include flexible conductors and sensors,[42] absorbents,[43] drug-releasing devices/needles,[44] and cell culture scaffolds.[45–47] In these studies, porous structures were prepared using sacrificial templates such as microparticles or emulsion droplets, which were first incorporated into the PDMS prepolymer and finally removed after crosslinking the PDMS. If microchambers were to be created using porous PDMS with interconnected pores as the substrate, a vertical flow of the culture medium through the microchambers could be realized, enabling the direct supply of the medium component to the spheroids. Such microchambers would also facilitate the creation of biocompatible, cost-effective, autoclavable, and highly replicable PDMS-based microfluidic devices. However, to the best of our knowledge, cell-culture microfluidic devices with integrated microchambers in porous PDMS substrates have not been developed. In particular, a process of forming microchambers, which are integrated with the channel structure, in a porous substrate by molding would be required, but there are no reports on such a process. Microchambers having a bottom plane composed of polymeric microporous membranes have recently been reported,[36] but the process of device fabrication needs to be refined in terms of the integration and stability of ultrathin membranes.

We here propose the concept of a porous microchamber-implementing microfluidic device, as shown in Fig. 1. In this device, relatively large-sized microchambers (φ of 300 μm) that are connected to the inlet channel are formed in the porous PDMS substrate. In contrast, relatively small-sized micropores (3–5 μm) are formed on the chamber surface; these do not allow the introduced cells to enter the pores, whereas the medium flows through the chamber to the outlet channel. The porous matrix was created *via* a salt-leaching process combined with centrifugation-assisted molding. Because the device was entirely composed of PDMS (or silicone), this seamless configuration ensures reliable operation and perfusion culture even under pressure application. This device vertically supplies the culture medium to the spheroids through the microchambers with the help of the continuous micropores. We expected that the liquid film surrounding the spheroids would become dramatically thinner, enhancing the diffusion-based transport of oxygen/nutrients to the cells in the chambers. We experimentally validated the effectiveness of this device by using it to form spheroids of cultured human hepatocytes (HepG2 cells), which are the often used cells in drug evaluation. We then compared the cell viability, proliferation ability, and functions in the vertical-flow chambers to those in conventional non-porous microchambers with horizontal flows and those in 2D plate culture.

Materials and methods

Design of the microdevice with porous microchambers

The detailed design of the microdevice is shown in Fig. 2(a) and (b). This device was composed of three layers: top and bottom PDMS plates (thickness of ~2 mm) with microchannel structures, and a middle silicone sheet (thickness of 1 mm) with a porous PDMS region with an embedded array of 271 microchambers with an opening and inner diameter of ~300/~230 μm, respectively. Using this microchamber we expected that spheroids with a diameter of less than ~200 μm are formed; this spheroid size corresponds to those in most previous studies and could prevent the formation of necrotic cores.[30] The width of the inlet/outlet channels was 700 μm, and the channel width at the chamber region was 9 mm. The microchannel depth was uniform at ~200 μm. There was one inlet and two outlets; the outlet for the inlet channel served as a drain for cell inoculation.

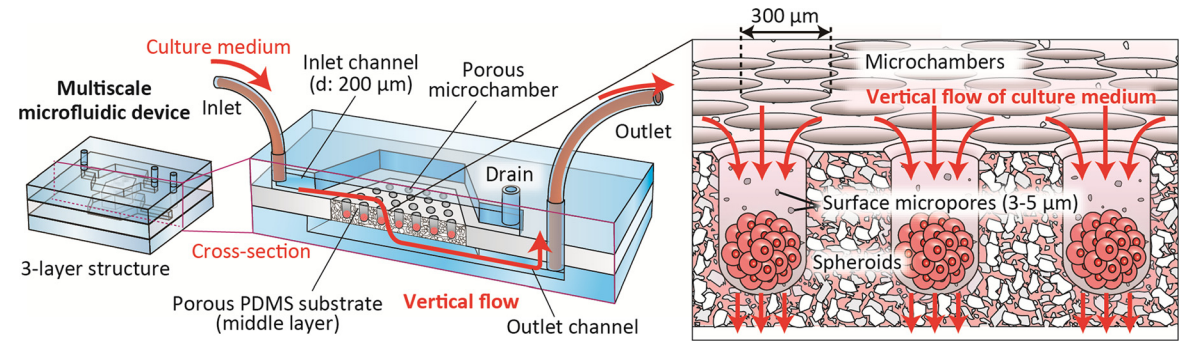

Fig. 1 Schematic image of the multiscale microfluidic device integrated with porous microchambers.

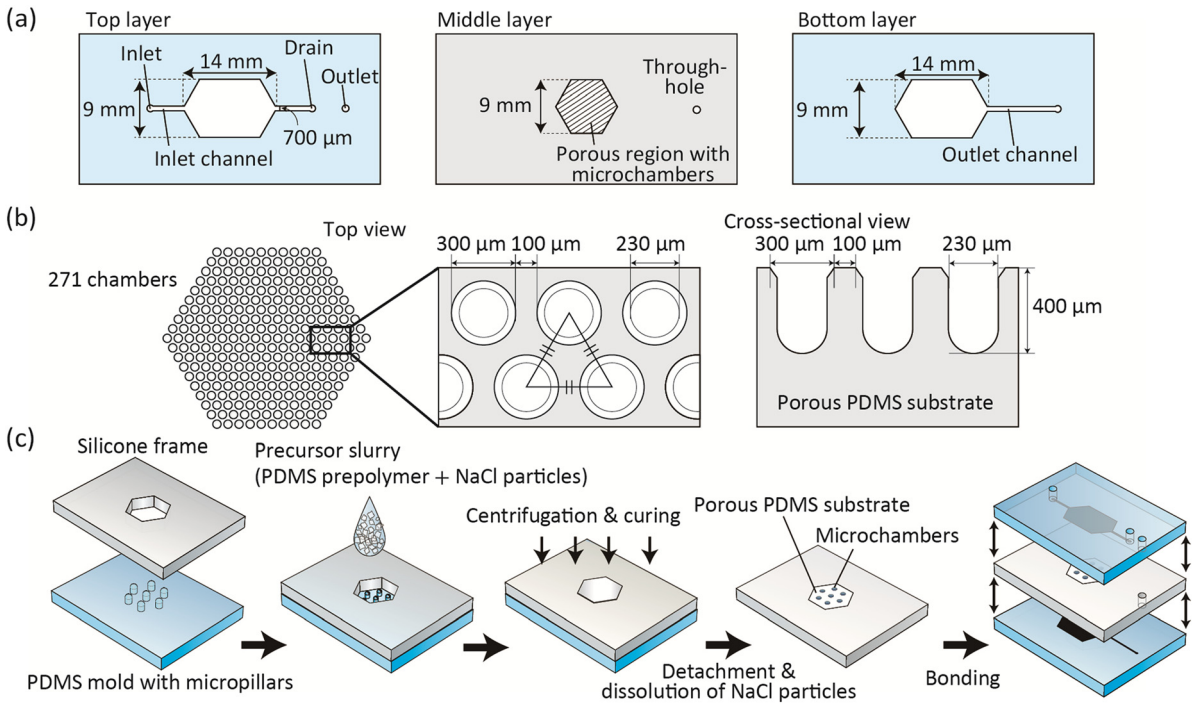

Fig. 2 (a and b) Designs of the microfluidic device composed of three layers: (a) microchannel designs and the porous region on the three layers composing the device and (b) design of the 271 microchambers on the upper surface of the middle layer. The middle layer was sandwiched between the top and bottom layers with microchannel structures. (c) Fabrication process of the porous microchambers and the microfluidic device.

Microdevice fabrication

The fabrication process of the microdevice is shown in Fig. 2(c). We proposed a salt-leaching process combined with the centrifugation-assisted replica molding to form the middle layer with the porous microchambers. As sacrificial particles (porogen), we employed NaCl particles with a diameter of 30–60 μm (NACL-UM; Naikai Salt, Okayama, Japan). Before their use in experiments, the NaCl particles were filtered through a woven wire mesh sieve with a mesh opening size of 100 μm to remove large aggregates. The base and the curing agent of the PDMS prepolymer (Silpot 184; Dow Corning Toray, Tokyo, Japan) were mixed at a ratio of 10 : 1. Then, the filtered NaCl particles were thoroughly mixed with the PDMS prepolymer using a planetary centrifugal mixer (AR-100; Thinky, Tokyo) for 2 min, and the precursor slurry was well degassed in a vacuum for 1–2 min. The volumetric mixing ratio of the NaCl particles in the precursor slurry was changed from 20% to 60%, with a corresponding weight ratio of ~35% to ~80%.

For the molding-based fabrication of the microchambers, a micromachined PMMA plate (Yasojima Proceed, Hyogo, Japan) was first obtained as the master mold with concave chamber structures. Then, the convex PDMS mold was prepared by the conventional replica molding process of PDMS against the master PMMA mold. The surface of the obtained PDMS mold with convex pillars was treated with O_2 plasma using a plasma reactor (PR500; Yamato Scientific,

Tokyo), and then immersed in methanol with 1% trimethoxy(1*H*,1*H*,2*H*,2*H*-heptadecafluorodecyl)silane (Tokyo Chemical Industry) for 30 min. Then, a silicone frame (thickness of 1 mm) with a hexagonal opening (width of 9 mm) was placed and fixed. The degassed precursor slurry was poured onto the PDMS mold and then centrifugal force was vertically applied using a plate centrifuge (PlateSpin3; Kubota, Tokyo) at 3500 rpm (1370 G) for 15 min. After curing at 85 °C for 150 min, the silicone frame with the crosslinked PDMS embedding the NaCl particles was detached from the mold, and then the backside of the porous PDMS substrate was made flat using a utility knife. Then, this plate was immersed in water at 70 °C overnight to dissolve the NaCl particles, and dried in an oven at 85 °C. The top and bottom PDMS layers were prepared using standard soft lithography and replica molding techniques using silicon/SU-8 molds. These three layers were bonded stepwise *via* O_2-plasma activation, with assembling of the microchannel/microchamber positions. Finally, inlet/outlet silicone tubes (inner and outer diameters of 1 and 2 mm, respectively) were inserted into the inlet/outlet ports and then glued.

In addition to the porous vertical-flow chambers, horizontal perfusion devices were fabricated to perform the control experiments. Microchambers were prepared on a non-porous PDMS plate using the same mold structure described above, and this microchamber plate was bonded with the top PDMS plate with the channel structure *via* O_2-plasma activation to form the 2-layer devices.

Characterization of the microdevice and the porous substrate

The pore connectivity of the porous PDMS substrate was evaluated by weighing the PDMS substrates before and after dissolving NaCl particles and by estimating the amount of NaCl particles eluted. The hydrodynamic resistance of the porous substrate was evaluated by introducing distilled water; the output flow rate was measured under the application of constant pressure using pressure control apparatus (My Flow HIP-240; Arbiotech, Tokyo) to the microdevice. The microscale morphology of the fabricated porous microchambers was observed using SEM (VE-8800; Keyence, Osaka, Japan); the top and cross-sectional morphologies were investigated. Additionally, the flow behaviors to and through the microchambers were investigated by introducing a suspension of fluorescent microparticles (green 1.1 μm particles (G0100) or red 3.2 μm particles (R0300); Thermo Fisher Scientific, MA, USA) in DI water and observing the particle movement using fluorescence microscopy (IX-73; Olympus, Tokyo) and a CCD camera (DP74; Olympus).

Perfusion culture of HepG2 cell spheroids

HepG2 cells (a human hepatoma cell line), kindly provided by Riken BRC (Ibaraki, Japan), were cultured in Dulbecco's modified Eagle's medium (DMEM; Fujifilm Wako Pure Chemical, Osaka, Japan) supplemented with 1% fetal bovine serum (FBS; Thermo Fisher), 100 U mL^{-1} penicillin and 0.1 mg mL^{-1} streptomycin (Sigma-Aldrich, St. Louis, MO, USA) at 37 °C with 5% CO_2 in a CO_2 incubator. Cells were harvested from cell culture dishes at 80–90% confluency by trypsin–EDTA (Sigma-Aldrich) treatment. The harvested cells were centrifuged and re-suspended in the culture medium at a density of 1×10^7 cells per mL. Before introducing cells, the microchannel was filled with saline to remove air from the porous substrate. An aliquot of this cell suspension (~100 μL) was introduced into the microchannel from the inlet. After 3 min of incubation, at which time point the introduced cells were precipitated on the bottom of the chamber, ~500 μL of the culture medium not containing cells was introduced to wash the cells on the microchannel floor away from the drain. The outlet was closed and the drain was opened, and the perfusion culture was performed overnight at a flow rate of 0.5 μL min^{-1}. After forming spheroids, the drain was closed and the outlet was opened, and perfusion culture was continued for up to 14 days. To characterize the spheroids off-chip, the chamber region of the device was cut out using a utility knife and the spheroids in the chamber were collected by centrifugation at 1000 rpm (180 G) for 5 min.

Measurement of the spheroid size

The size of the spheroids was measured from the optical micrographs of the collected spheroids captured using an optical/fluorescence microscope. The long and short axes were measured using the ImageJ software (NIH, MD) and these values were averaged. At least 20 spheroids were analyzed for each condition.

Cell viability assay, H&E staining, and immunohistochemistry

Cell viability was assessed using a live/dead viability kit (Thermo Fisher) based on the manufacturer's instruction. The live and dead cells were stained green and red, respectively. For histochemical analysis of the spheroids, thin paraffin sections of the spheroids at day 7 were prepared (thickness of 7 μm). For the HE (hematoxylin and eosin) staining, prepared sections were stained with hematoxylin and eosin. Immunohistochemical analysis of Ki-67, a nuclear protein used as a marker for proliferative cells, was also performed. After chemical fixation with 1% antigen retrieval buffer (100× citrate buffer, pH 6.0; Abcam, Cambridge, UK), the sample was blocked with 10% donkey serum in PBS for 30 min, followed by incubation with an anti-Ki-67 rabbit monoclonal antibody (Abcam) at 4 °C overnight. The sections were incubated with goat anti-rabbit IgG H&L (Alexa Fluor 594; Thermo Fisher) for 30–60 min. Finally, the sections were mounted using a ProLong gold antifade reagent with DAPI (Thermo Fisher). The ratios of the Ki-67-positive cells were evaluated from ~150–300 cells in 5 randomly selected images (n = 4–5).

Real-time quantitative reverse transcription PCR (RT-qPCR)

The expression levels of hepatocyte-specific genes of HepG2 cells were examined using RT-qPCR. The spheroids under the

vertical and horizontal-flow conditions at day 14 and the cells cultured using a conventional 2D plate culture at 80–90% confluency were examined. From these samples, the total RNA was isolated using a TRIzol reagent (Thermo Fisher) and purified using a Pure Link RNA mini kit (Thermo Fisher). Genomic DNA was removed using DNase I (Thermo Fisher). Complementary DNA was synthesized from 300 ng of total RNA using a SuperScript IV VILO reverse transcriptase (Thermo Fisher). RT-qPCR analysis was performed with a TaqMan master mix (Thermo Fisher) using a Step One Plus Real-Time PCR System (Thermo Fisher). The expression levels of the following genes were evaluated using TaqMan probes and primers (Thermo Fisher): albumin (ALB, Hs00609410_m1), ornithine transcarbamylase (OTC, Hs00166892_m1), cytochrome P450 1A2 (CYP1A2, Hs00167927_m1), cytochrome P450 3A4 (CYP3A4, Hs00604506_m1), and GAPDH (Hs99999905_m1). The relative expression levels of ALB and OTC were quantified using the comparative CT method and normalized to the expression levels of GAPDH as the housekeeping control. The gene expressions of the control 2D plate culture samples were normalized to 1.

Statistical analysis

The obtained data were statistically analyzed by Student's *t*-test or by one-way analysis of variance (ANOVA) with the Bonferroni or Games–Howell *post hoc* test using the IBM SPSS Statistics 22 software (IBM Japan, Tokyo). A p value less than 0.05 was considered statistically significant.

Results and discussion

Fabrication of porous microchambers

The first step in the successful development of a vertical-flow perfusion system was to establish a method for the formation of porous microchambers using the newly developed molding process. We employed PDMS as the material for the chambers because the liquid-state PDMS prepolymer enables the uniform incorporation of fine particles that function as porogens and can then be molded and crosslinked into the desired shape. Additionally, PDMS can be seamlessly and firmly bonded with another silicon-based plate made of glass, Si wafers, and silicone/PDMS, through the simple process of O_2 plasma-based activation. NaCl particles were used as the porogens because of their low cost, available size variation, high solubility in water, and low cytotoxicity even with some residuals. Regarding particle size, we used 30–60 μm NaCl particles; when particles smaller than this were employed, the viscosity of the precursor slurry became too high, making it difficult to manipulate.

First, the ratio of the NaCl particles was investigated to find the optimum fabrication conditions. This is because a low particle ratio may result in isolated NaCl particles that are not dissolved and may not function as porogens. The ratio of the dissolved NaCl particles was examined by weighing the polymer matrices before and after dissolving the NaCl particles. As shown in Fig. 3(a), when the ratio was 35% or lower, the dissolution ratio did not reach 100%. This indicates that some undissolved NaCl particles remained in the PDMS substrate. On the other hand, when the ratio was equal to or greater than 40%, the incorporated particles were completely dissolved. Under these conditions, it was expected that almost all the introduced NaCl particles were in contact with other NaCl particles in the precursor, thereby generating continuous pores inside the PDMS substrate. In the next experiment, the ratio was changed from 40% to 50%; the precursor slurry with a particle concentration higher than 55% was also difficult to manipulate because of its high viscosity.

We then fabricated microchambers using a mold with convex pillars. When the degassed precursor slurry was applied to the opening of the silicone frame and crosslinked without the centrifugation process, large holes were formed on the surface of the microchambers (ESI† Fig. S1). This was because air bubbles, trapped on the mold surface, could not be removed from the precursor even by degassing. Therefore, we employed the centrifugation process; the precursor mixture was firmly pressed against the mold by centrifugation to remove the trapped air. The porous part was firmly attached and fixed to the silicone frame. We confirmed that centrifugation for 15 min resulted in the formation of a relatively smooth microchamber surface with small pores, when the ratio of the NaCl particles was 50% (v/v) (Fig. S1†). In the preparation of porous PDMS, there are mainly two methods: one is the use of particles, and the other is the use of droplets as porogens. Since this study combines molding and centrifugal operations, the method using emulsion droplets should probably not be applicable, and the method using solid particles as porogens is considered suitable.

SEM images of the cross-section and the top view of the microchambers obtained under a 50% (v/v) NaCl concentration condition are shown in Fig. 3(b). In the cross-section, there are many pores that were possibly interconnected. No inhomogeneity or orientation of the internal pores was observed, and the pores were uniformly formed in the entire cross section. The size of the pores on the microchamber surface was typically in the range of 2–5 μm, with a density of ~100 ± 20 pores per chamber (Fig. S2†). This pore size was considered to be smaller than typical mammalian cells (~10 μm), which would be suitable to retain the introduced cells in the chamber. It was interesting to see that the number of pores formed on the upper surface of the porous PDMS substrate was very limited. This may have been because, at the time of centrifugation, the NaCl particles did not precipitate into the region near the bottom surface of the mold, but merely precipitated onto the pillar surface. To the best of our knowledge, this study is the first report documenting the combination of the molding-based fabrication of microchambers in a porous matrix with smaller-sized continuous pores, an approach made possible by the application of centrifugal force to a highly viscous precursor slurry. Although a recent study described the use of

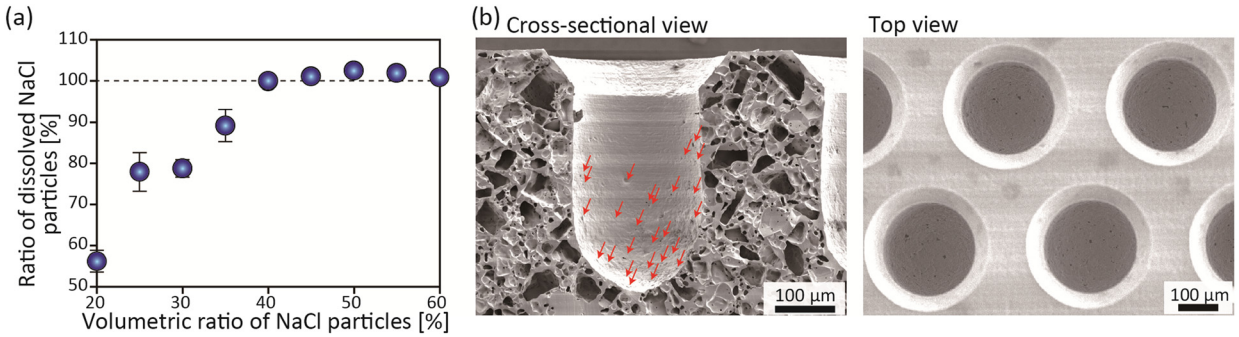

Fig. 3 (a) Relationship between the volumetric ratio of NaCl particles in the precursor slurry and the ratio of the dissolved NaCl particles. (b) Scanning electron microscopy observation of the cross section and the surface of the porous microchambers. Red arrows in the left panel indicate micropores on the surface of the microchambers.

a track-etched membrane for the formation of spheroids,[36] that study employed pre-prepared porous membranes that are not compatible with seamless integration with PDMS-based microchannels. In the present study, we created one-piece devices made entirely of PDMS or silicone, including the tube connections. The devices could therefore resist fluid leakage and were autoclavable. These characteristics could be achieved by our newly proposed method, which combines replica molding and salt leaching for PDMS. Due to these advantages, the presented fabrication protocol is expected to become a new approach to creating versatile, multiscale microfluidic devices. It should be noted that the shape of the NaCl particles was irregular (Fig. S3†), which may have been why the surface pores were not uniform in shape. The surface pores were thought to have formed where the corners of the irregularly shaped particles and the substrate at the bottom came into contact. The use of particles of more uniform shape and size would facilitate the formation of more uniform pores.

Characterization of the microdevice

The obtained plate with the porous region containing microchambers was then sandwiched between the top/bottom microchannel plates to form the three-layered, multiscale microfluidic devices, as shown in Fig. 4(a). Prior to performing the perfusion culture of cells, we evaluated the fluid performance of the device, including the connectivity of the pores, the flow resistances of the porous matrix, and the uniformity in flow distribution. First, distilled water was introduced into the device while controlling the applied pressure. The flow rate through the device was measured to evaluate the flow resistance, which is one of the key parameters possibly affecting the cells in the perfusion experiment. Microdevices prepared using a 45% or 50% volumetric mixing ratio of NaCl particles were tested. The relationship between the applied pressure and the volumetric flow rate is shown in Fig. 4(b). The introduced water flowed through the porous region and was collected from the outlet, indicating that the micropores inside the porous matrix were actually interconnected. The flow rate under the 50% condition was ~1.5 times higher than that under the 45% condition when the same pressure was applied. Since we have already confirmed that almost all of the introduced NaCl particles were dissolved under these conditions (Fig. 3(b)), it was assumed that the contact points between the NaCl particles increased when the volumetric mixing ratio of the NaCl particles was increased from 45% to 50%. Since the perfusion culture was performed at a flow rate of 0.5 μL min^{-1}, the pressure values exerted on the cells by the perfusion were expected to be far less than 1 kPa. This value is sufficiently lower than the blood pressure and would not cause damage to the cells.

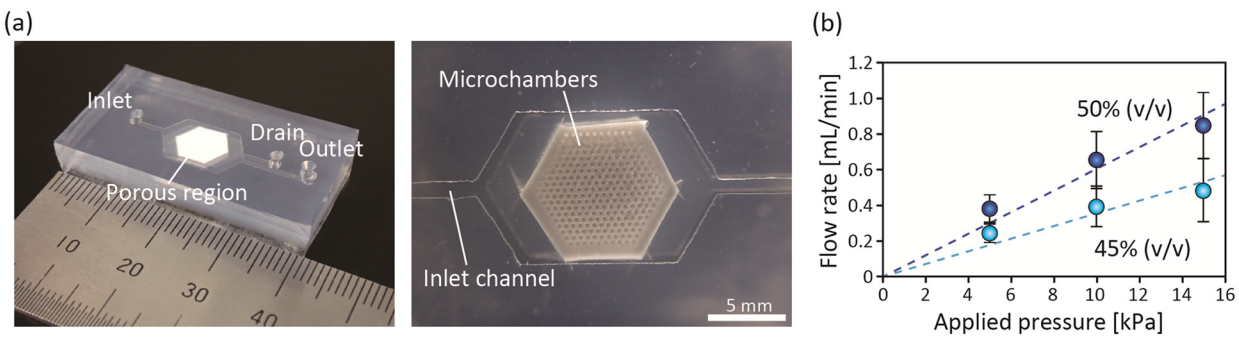

Fig. 4 (a) Photograph of the fabricated microdevice; (left) the entire microchannel and (right) porous PDMS region. (b) Examination of the resistance of the flow of DI water through the device. The relationship between the applied pressure and the flow rate is shown for the devices prepared by using a 45% or 50% volumetric ratio of NaCl particles.

Another critical factor dominating the success of perfusion is the uniformity in flow distribution to all microchambers, because there were variations in the number, shape, and size of the surface pores of the chambers. A microdevice prepared at a 50% ratio was tested, and distilled water with 1.1 μm green fluorescent particles as a tracer was introduced into the device. The behavior of the tracer particles flowing into the chambers was observed by fluorescence microscopy. The results are shown in ESI† Movie S1. Although we did not quantitatively analyze the number of particles flowing through each microchamber, we confirmed that flows were generated through all of the microwells. This was because ~100 micropores were formed on the microchamber surface, indicating the relatively high uniformity and reproducibility of the fabrication of the multiscale microdevice. It should be noted that 3.2 μm particles did not flow through the porous matrix but were just retained in the chamber. In the following cell culture experiment, we employed devices created at a volumetric mixing ratio of 50%.

In addition to the porous microchambers with a vertical flow, we employed non-porous chambers with a horizontal flow as a control. For the non-porous chambers, we conducted an experiment to introduce 1.1 μm tracer particles as a comparison (Fig. S4†). As a result, the flow reached only ~1/3 of the chamber depth from the surface. This result indicates the superiority of the porous chambers because the medium flow can be supplied directly to the entire region of the chamber, and there is no need to consider the inhomogeneity of the oxygen/nutrient supply depending on the upstream/downstream positions of the chambers.

Perfusion culture of HepG2 cell spheroids

We next performed perfusion culture of mammalian cells and examined the effects of the presented device on the function/viability of the spheroids. In this study, we used HepG2 cells, a human hepatoma cell line that is often used in drug assays,[48–50] especially because it retains some of the metabolic functions of native hepatocytes. It has been reported that the formation of spheroids of HepG2 cells upregulates the expressions of hepatocyte-specific functions.[51] However, in spheroids larger than ~300 μm, the core becomes necrotic in a static culture.[30] In the present study, we employed microchambers with an inner diameter of ~230 μm to form spheroids with a diameter of ~200 μm and investigated the effects of the direct supply of medium components by the vertical flow on the functions of HepG2 cell spheroids. In this experiment, perfusion culture was performed at 0.5 μL min^{-1}, which corresponds to an average vertical flow velocity of 0.74 μm s^{-1} in the 230 μm diameter chamber. In addition, HepG2 cells did not adhere to the PDMS surface, although no surface treatment was applied.

We tested both the porous microchambers with a vertical flow and non-porous chambers with a horizontal flow (control). After introducing cells and culturing them, we collected the formed spheroids from the device and determined the spheroid size. As shown in Fig. 5, the spheroid size at day 1 was uniformly ~150 μm for these two types of devices, indicating that the number of cells introduced into the chambers was uniform and the manipulation was reproducible. During perfusion culture, the cells in the spheroids gradually proliferated and the spheroid size increased. The vertical-flow condition promoted cell proliferation compared to the horizontal flow, although the difference was not great. At day 7, the spheroid diameters were increased to ~1.3-fold and ~1.5-fold of those at day 1, for the horizontal-flow and vertical-flow conditions, respectively. This difference may have been due to the more efficient and direct supply of oxygen and nutrients to the spheroids in the vertical-flow culture.

Cell viability assay, HE staining, and immunohistochemistry of Ki-67

To further investigate whether cellular functions other than spheroid size were altered under the vertical/horizontal flow conditions, we next assessed the cell viability in the

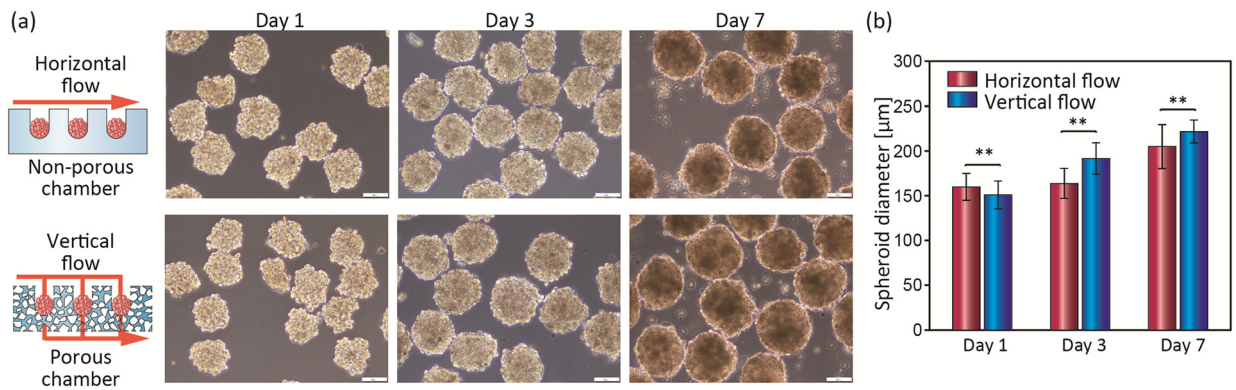

Fig. 5 (a) Micrographs of the spheroids formed under both the horizontal-flow and vertical-flow conditions and collected from the device at days 1, 3, and 7. Scale bar, 100 μm. (b) Time course change in the spheroids under the horizontal-flow and vertical-flow conditions. Data are the mean ± SD of at least 30 spheroids. $^{**}p < 0.01$.

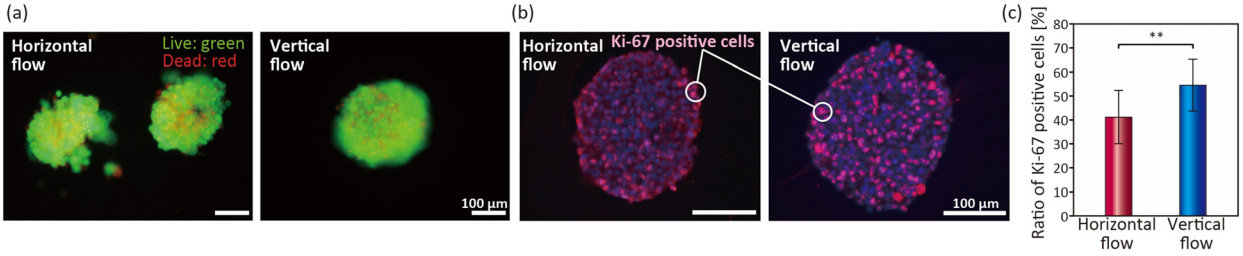

Fig. 6 (a) Live/dead cell viability assay for spheroids under the horizontal-flow and vertical-flow conditions at day 10. Viable and non-viable cells were stained green and red, respectively. (b) Immunohistochemistry of the Ki-67-positive cells in the cross sections of the spheroids cultured under the horizontal-flow and vertical-flow conditions at day 7. Ki-67-positive cells and cell nuclei were stained red and blue, respectively. (c) Quantification of Ki-67-positive cells. Values are the mean ± SD of 15 (horizontal flow) or 20 (vertical flow) spheroids.

spheroids at day 10. As shown in Fig. 6(a), the cell viability examined by the live/dead assay was maintained at >90% under both conditions. This result indicates that even the horizontal-flow condition in the non-porous chambers was not severe for the cells, primarily owing to the relatively small size of the spheroids formed (~200 μm). This result is consistent with previous reports that spheroids of ~200 μm are not sufficiently large to develop necrotic cores.[52–54] The results of HE staining showed that the cells in the spheroids are interconnected, but no significant differences between these two conditions were observed (Fig. S5†).

To directly confirm whether the proliferative potential of the cells is altered, immunohistochemical staining of Ki-67, a nuclear protein associated with cell proliferation,[55] was performed. The results of the double staining of the Ki-67-positive cells (red) and cell nuclei (blue) at day 7 are shown in Fig. 6(b). Under the horizontal-flow condition, the ratio of the Ki-67-positive cells was not high near the center region of the spheroids. In contrast, the Ki-67-positive cells were evenly distributed in the spheroids cultured under the vertical-flow condition, indicating that the cells even near the center of the spheroids were proliferating. From the quantitative evaluation, the ratio of the Ki-67-positive cells under the vertical-flow condition (~55%) was higher than that under the horizontal-flow condition (~40%). It was previously reported that a limited oxygen supply to spheroids resulted in the poor proliferation ability of cells.[56] Our results therefore suggested that the use of vertical flow to directly supply the medium to the spheroids prevented the formation of stagnant flow regions, thereby preventing the deprivation of oxygen.

Gene expression analysis

For the biomedical and pharmaceutical applications of the spheroids, it would be desirable to maintain or upregulate the organ/tissue-specific functions of cells in the *in vitro* culture platforms. We therefore analyzed the expressions of representative genes of hepatic cells, including albumin (ALB), a serum protein, and ornithine transcarbamylase (OTC), an enzyme involved in urea synthesis, both of which are often used as indicators of hepatic functions.[22,57,58] We also investigated the expressions of two cytochrome P450 enzymes, CYP1A2 and CYP3A4, which are the most common enzymes for drug metabolization.[59] The spheroids under horizontal-flow and vertical-flow conditions on day 14 and on conventional 2D plate culture at 80% confluency, as a control, were examined by RT-qPCR. The results are shown in Fig. 7. The expression level of ALB in the horizontal flow was nearly equivalent to that in the 2D plate culture, but the ALB expression level under the vertical-flow condition was higher than those under the plate culture and the horizontal-flow conditions. The expression of OTC under the vertical-flow condition was the highest among these conditions. Previous studies have reported that these functions of HepG2 cells are associated with the efficiency of the medium supply,[39,60,61] and are also controlled by the spheroid size and perfusion flow rate. Hence, these results indicated that the medium component is efficiently supplied to the cells under the vertical-flow condition. On the other hand, under the horizontal flow condition, the tracer particle results (Fig. S3†) indicated that the streamlines reached only ~1/3 of the depth of the chamber, so it was assumed that the diffusion-based oxygen and nutrient supply was insufficient. In general, there is a trade-off between the cell proliferation and the expression of cellular functions, with proliferating cells

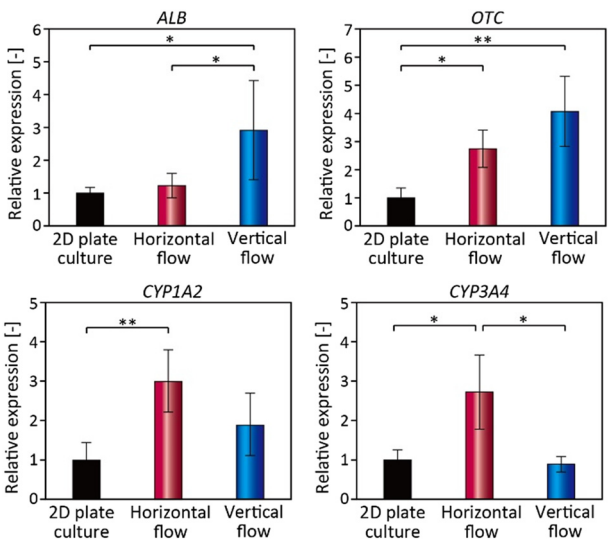

Fig. 7 Gene expression analysis of HepG2 cells in 2D plate culture and spheroids in the horizontal-flow and vertical-flow devices. ALB: albumin; OTC: ornithine transcarbamylase; CYP: cytochrome P450.

tending to have a lower expression of cellular functions. The spheroids cultured under the vertical-flow condition showed an improvement in proliferative ability, but also exhibited an upregulation of cellular functions, including albumin and OTC expressions. This remarkable characteristic would be attributed to the direct supply of the culture medium to the proximity of the spheroids.

The expressions of the two CYP genes, on the other hand, were the highest under the horizontal-flow condition. It has been reported that the expression of CYP family members is decreased in HepG2 cells cultured under higher O_2 tension conditions.[60,62] This is because the physiological O_2 tension varies depending on the location of hepatocytes in the liver, which has the effect of regulating the zone-specific expressions of functions. Indeed, in the liver, the expression of the CYP family is localized near the central vein, where the O_2 tension is lower (30–35 mmHg) than that near the portal vein (60–65 mmHg).[63] From this viewpoint, our results on CYP expression suggested that the O_2 supply was enhanced under the vertical-flow condition. Therefore, it might be possible to maximize the target cell functions associated with O_2 tension and/or specific growth factors simply by controlling their initial concentrations. In this study, we just tested a cultured hepatocyte cell line. Because primary hepatocytes may even be more useful for hepatotoxicity evaluation systems in drug discovery,[64] and hence, validations using other types of cells would be highly beneficial.

Conclusions

We have developed a new concept for spheroid culture using a vertical-flow perfusion system featuring multiscale microfluidic devices with porous microchambers. A process combining centrifugation-assisted molding and a salt-leaching technique was proposed to create microchambers embedded in a porous PDMS substrate, which enables subsequent seamless integration of the chambers into a microfluidic device. We were able to retain the introduced cells in the chambers, while the culture medium is directly supplied through the porous PDMS substrate with continuous micropores. Owing to the direct and vertical medium flow, the thickness of the liquid film surrounding the spheroids was considered to be decreased, improving the diffusion-based transport of oxygen, nutrients, and metabolic waste to the spheroids. Consequently, we showed that spheroids cultured using this system exhibited enhanced cell proliferation even at the center of the spheroids, as demonstrated by Ki-67 staining. Hepatocyte-specific functions were also regulated compared to the conventional horizontal-flow condition and 2D plate culture. We expect that the presented device will upgrade the spheroids culture platforms with medium perfusion, because the efficient supply and control of oxygen/nutrients would be suitable for maximizing the cell function, proliferation, and viability. Because of its effectiveness and versatility, the presented system can be applied to cell-based drug development and in a variety of biomedical research applications. In this study, the size of the spheroids was ~200 μm, and the conditions were such that necrotic cores were not formed. In the next step, it will be necessary to investigate whether the formation of necrotic cores can be prevented for much larger spheroids. Additionally, it would be beneficial to examine whether the presented device can be applied to the cell culture systems that mimic an anaerobic environment, such as cancer cell spheroids.

Author contributions

Conceptualization: MT, MY, and RU; writing – original draft preparation: MT and MY; writing – review & editing: MT, MY, and RU; visualization: MT and MY; Supervision: RU and MS.

Conflicts of interest

There are no conflicts to declare.

Acknowledgements

This study was supported in part by the Grants-in-aid for Scientific Research (20H02529, 18K18969, and 22H01875) from the Ministry of Education, Culture, Sports, Science, and Technology, Japan. We thank Naikai Salt for kindly supplying the NaCl particles and Mr. Aruto Hori at Chiba University for technical assistance.

References

1 K. Moshksayan, N. Kashaninejad, M. E. Warkiani, J. G. Lock, H. Moghadas, B. Firoozabadi, M. S. Saidi and N. T. Nguyen, *Sens. Actuators, B*, 2018, **263**, 151–176.
2 S. J. Kim, E. M. Kim, M. Yamamoto, H. Park and H. Shin, *Adv. Healthcare Mater.*, 2020, **7**, 1701165.
3 H. Shen, S. Cai, C. Wu, W. Yang, H. Yu and L. Liu, *Micromachines*, 2021, **12**, 96.
4 J. Ro, J. Kim and Y. K. Cho, *Analyst*, 2022, **147**, 2023–2034.
5 G. Pettinato, R. Ramanathan, R. A. Fisher, M. J. Mangino, N. Zhang and X. Wen, *Sci. Rep.*, 2016, **6**, 32888.
6 N. E. Ryu, S. H. Lee and H. Park, *Cell*, 2019, **8**, 1620.
7 S. Sant and P. A. Johnston, *Drug Discovery Today: Technol.*, 2017, **23**, 27–36.
8 S. A. Langhans, *Front. Pharmacol.*, 2018, **9**, 6.
9 K. P. Kanebratt, A. Janefeldt, L. Vilen, A. Vildhede, K. Samuelsson, L. Milton, A. Bjorkbom, M. Persson, C. Leandersson, T. B. Andersson and C. Hilgendorf, *J. Pharm. Sci.*, 2021, **110**, 422–431.
10 R. Z. Lin, L. F. Chou, C. C. Chien and H. Y. Chang, *Cell Tissue Res.*, 2006, **324**, 411–422.
11 A. Jaukovic, D. Abadjieva, D. Trivanovic, E. Stoyanova, M. Kostadinova, S. Pashova, S. Kestendjieva, T. Kukolj, M. Jeseta, E. Kistanova and M. Mourdjeva, *Stem Cell Rev. Rep.*, 2020, **16**, 853–875.
12 K. Bialkowska, P. Komorowski, M. Bryszewska and K. Milowska, *Int. J. Mol. Sci.*, 2020, **21**, 6225.

13 D. Huang, X. Zhang, X. Fu, Y. Zu, W. Sun and Y. Zhao, *Engineered Regeneration*, 2021, **2**, 246–256.
14 Y. Ichihara, R. Utoh, M. Yamada, T. Shimizu and Y. Uchigata, *Heliyon*, 2016, **2**, e00129.
15 M. E. Boutin, L. L. Kramer, L. L. Livi, T. Brown, C. Moore and D. Hoffman-Kim, *J. Neurosci. Methods*, 2018, **299**, 55–63.
16 S. Mattapally, W. Zhu, V. G. Fast, L. Gao, C. Worley, R. Kannappan, A. V. Borovjagin and J. Zhang, *Am. J. Physiol.*, 2018, **315**, H327–H329.
17 F. Itel, J. Skovhus Thomsen and B. Stadler, *ACS Appl. Mater. Interfaces*, 2018, **10**, 30180–30190.
18 F. G. Torizal, K. Kimura, I. Horiguchi and Y. Sakai, *Regener. Ther.*, 2019, **12**, 66–73.
19 Y. Du, N. Li, H. Yang, C. H. Luo, Y. X. Gong, C. F. Tong, Y. X. Gao, S. Q. Lu and M. Long, *Lab Chip*, 2017, **17**, 782–794.
20 T. Kageyama, L. Yan, A. Shimizu, S. Maruo and J. Fukuda, *Biomaterials*, 2019, **212**, 55–63.
21 J. Lee, S. Lee, S. J. Huh, B. J. Kang and H. Shin, *Adv. Sci.*, 2022, **9**, e2103525.
22 M. Yamada, A. Hori, S. Sugaya, Y. Yajima, R. Utoh, M. Yamato and M. Seki, *Lab Chip*, 2015, **15**, 3941–3951.
23 R. Utoh, S. Enomoto, M. Yamada, K. Yamanaka, Y. Yajima, K. Furusawa and M. Seki, *Mater. Sci. Eng., C*, 2021, **129**, 112417.
24 A. Morita, M. Yamada, R. Utoh, K. Momiyama, H. Iwadate and M. Seki, *J. Biosci. Bioeng.*, 2022, **133**, 265–272.
25 B. S. Jang, K. H. Park, E. Y. Suh, B. S. Lee, S. W. Kang and K. M. Huh, *Int. J. Biol. Macromol.*, 2021, **187**, 955–963.
26 C. Shao, Y. Liu, J. Chi, Z. Chen, J. Wang and Y. Zhao, *Langmuir*, 2019, **35**, 3832–3839.
27 H. Ota, R. Yamamoto, K. Deguchi, Y. Tanaka, Y. Kazoe, Y. Sato and N. Miki, *Sens. Actuators, B*, 2010, **147**, 359–365.
28 Y. Markovitz-Bishitz, Y. Tauber, E. Afrimzon, N. Zurgil, M. Sobolev, Y. Shafran, A. Deutsch, S. Howitz and M. Deutsch, *Biomaterials*, 2010, **31**, 8436–8444.
29 J. Fukuda and K. Nakazawa, *Biomicrofluidics*, 2011, **5**, 22205.
30 T. Anada, J. Fukuda, Y. Sai and O. Suzuki, *Biomaterials*, 2012, **33**, 8430–8441.
31 S. Daster, N. Amatruda, D. Calabrese, R. Ivanek, E. Turrini, R. A. Droeser, P. Zajac, C. Fimognari, G. C. Spagnoli, G. Iezzi, V. Mele and M. G. Muraro, *Oncotarget*, 2017, **8**, 1725–1736.
32 D. A. Close and P. A. Johnston, *SLAS Discovery*, 2022, **27**, 39–54.
33 G. Lee, Y. Jun, H. Jang, J. Yoon, J. Lee, M. Hong, S. Chung, D. H. Kim and S. Lee, *Acta Biomater.*, 2018, **65**, 185–196.
34 H. Mihara, M. Kugawa, K. Sayo, F. Tao, M. Shinohara, M. Nishikawa, Y. Sakai, T. Akama and N. Kojima, *Cell*, 2019, **8**, 525.
35 E. Fennema, N. Rivron, J. Rouwkema, C. van Blitterswijk and J. de Boer, *Trends Biotechnol.*, 2013, **31**, 108–115.
36 T. T. Tao, Y. Q. Wang, W. W. Chen, Z. Y. Li, W. T. Su, Y. Q. Guo, P. W. Deng and J. H. Qin, *Lab Chip*, 2019, **19**, 948–958.
37 S. A. Lee, Y. Noda, E. Kang, J. Ju, D. S. Kim and S. H. Lee, *Lab Chip*, 2013, **13**, 3529–3537.
38 Y. Jun, J. Lee, S. Choi, J. H. Yang, M. Sander, S. Chung and S. H. Lee, *Sci. Adv.*, 2019, **5**, eaax4520.
39 L. D. Ma, Y. T. Wang, J. R. Wang, J. L. Wu, X. S. Meng, P. Hu, X. Mu, Q. L. Liang and G. A. Luo, *Lab Chip*, 2018, **18**, 2547–2562.
40 Y. Sakai, K. Hattori, F. Yanagawa, S. Sugiura, T. Kanamori and K. Nakazawa, *Biotechnol. J.*, 2014, **9**, 971–979.
41 D. Y. Zhu, S. Handschuh-Wang and X. C. Zhou, *J. Mater. Chem. A*, 2017, **5**, 16467–16497.
42 J. Hwang, Y. Kim, H. Yang and J. H. Oh, *Composites, Part B*, 2021, **211**, 108607.
43 S. J. Choi, T. H. Kwon, H. Im, D. I. Moon, D. J. Baek, M. L. Seol, J. P. Duarte and Y. K. Choi, *ACS Appl. Mater. Interfaces*, 2011, **3**, 4552–4556.
44 L. Bao, J. Park, G. Bonfante and B. Kim, *Drug Delivery Transl. Res.*, 2022, **12**, 395–414.
45 J. Lee, M. J. Cuddihy, G. M. Cater and N. A. Kotov, *Biomaterials*, 2009, **30**, 4687–4694.
46 F. Tokito, M. Shinohara, M. Maruyama, K. Inamura, M. Nishikawa and Y. Sakai, *J. Biosci. Bioeng.*, 2021, **131**, 543–548.
47 R. Riesco, L. Boyer, S. Blosse, P. M. Lefebvre, P. Assemat, T. Leichle, A. Accardo and L. Malaquin, *ACS Appl. Mater. Interfaces*, 2019, **11**, 28631–28640.
48 B. Ma, G. Zhang, J. Qin and B. Lin, *Lab Chip*, 2009, **9**, 232–238.
49 J. Saito, A. Okamura, K. Takeuchi, K. Hanioka, A. Okada and T. Ohata, *Toxicol. In Vitro*, 2016, **33**, 63–70.
50 J. Xu, S. Oda and T. Yokoi, *Toxicol. In Vitro*, 2018, **48**, 286–301.
51 M. Ingelman-Sundberg and V. M. Lauschke, *Basic Clin. Pharmacol. Toxicol.*, 2022, **130**(S1), 5–15.
52 E. Curcio, S. Salerno, G. Barbieri, L. De Bartolo, E. Drioli and A. Bader, *Biomaterials*, 2007, **28**, 5487–5497.
53 W. Liu, J. Xu, T. Li, L. Zhao, C. Ma, S. Shen and J. Wang, *Anal. Chem.*, 2015, **87**, 9752–9760.
54 M. Barisam, M. S. Saidi, N. Kashaninejad and N. T. Nguyen, *Micromachines*, 2018, **9**, 94.
55 X. Sun and P. D. Kaufman, *Chromosoma*, 2018, **127**, 175–186.
56 A. Gomes, L. Guillaume, D. R. Grimes, J. Fehrenbach, V. Lobjois and B. Ducommun, *PLoS One*, 2016, **11**, e0161239.
57 Y. Yajima, C. N. Lee, M. Yamada, R. Utoh and M. Seki, *J. Biosci. Bioeng.*, 2018, **126**, 111–118.
58 K. Shibuya, M. Watanabe, R. Goto, M. Zaitsu, Y. Ganchiku and A. Taketomi, *Cell Transplant.*, 2021, **30**, 9636897211000014.
59 M. Martignoni, G. M. Groothuis and R. de Kanter, *Expert Opin. Drug Metab. Toxicol.*, 2006, **2**, 875–894.
60 T. Nishikawa, Y. Tanaka, M. Nishikawa, Y. Ogino, K. Kusamori, N. Mizuno, Y. Mizukami, K. Shimizu, S. Konishi, Y. Takahashi and Y. Takakura, *Biol. Pharm. Bull.*, 2017, **40**, 334–338.
61 D. Miyamoto, T. Hara, A. Hyakutake and K. Nakazawa, *J. Biosci. Bioeng.*, 2018, **125**, 729–735.
62 T. J. DiProspero, E. Dalrymple and M. R. Lockett, *Toxicol. In Vitro*, 2021, **74**, 105156.
63 T. Kietzmann, *Redox Biol.*, 2017, **11**, 622–630.

64 C. C. Bell, D. F. G. Hendriks, S. M. L. Moro, E. Ellis, J. Walsh, A. Renblom, L. Fredriksson Puigvert, A. C. A. Dankers, F. Jacobs, J. Snoeys, R. L. Sison-Young, R. E. Jenkins, Å. Nordling, S. Mkrtchian, B. Kevin Park, N. R. Kitteringham, C. E. P. Goldring, V. M. Lauschke and M. Ingelman-Sundberg, *Sci. Rep.*, 2016, **6**, 25187.